THE JOURNAL OF CHEMICAL PHYSICS **128**, 064511 (2008)

Nonequilibrium molecular dynamics simulations with a backward-forward trajectories sampling for multidimensional infrared spectroscopy of molecular vibrational modes

Taisuke Hasegawa[a] and Yoshitaka Tanimura
Department of Chemistry, Graduate School of Science, Kyoto University, Sakyoku, Kyoto 606-8502, Japan

(Received 29 October 2007; accepted 3 December 2007; published online 14 February 2008)

A full molecular dynamics (MD) simulation approach to calculate multidimensional third-order infrared (IR) signals of molecular vibrational modes is proposed. Third-order IR spectroscopy involves three-time intervals between three excitation and one probe pulses. The nonequilibrium MD (NEMD) simulation allows us to calculate molecular dipoles from nonequilibrium MD trajectories for different pulse configurations and sequences. While the conventional NEMD approach utilizes MD trajectories started from the initial equilibrium state, our approach does from the intermediate state of the third-order optical process, which leads to the doorway-window decomposition of nonlinear response functions. The decomposition is made before the second pump excitation for a two-dimensional case of IR photon echo measurement, while it is made after the second pump excitation for a three-dimensional case of three-pulse IR photon echo measurement. We show that the three-dimensional IR signals are efficiently calculated by using the MD trajectories backward and forward in time for the doorway and window functions, respectively. We examined the capability of the present approach by evaluating the signals of two- and three-dimensional IR vibrational spectroscopies for liquid hydrogen fluoride. The calculated signals might be explained by anharmonic Brownian model with the linear-linear and square-linear system-bath couplings which was used to discuss the inhomogeneous broadening and dephasing mechanism of vibrational motions. The predicted intermolecular librational spectra clearly reveal the unusually narrow inhomogeneous linewidth due to the one-dimensional character of HF molecule and the strong hydrogen bond network. © *2008 American Institute of Physics*. [DOI: 10.1063/1.2828189]

I. INTRODUCTION

Multidimensional vibrational spectroscopies, whose spectra are obtained by recording the signals as a function of the time durations between the trains of pulses, have the potential to reveal the detailed static and dynamical features of molecular interactions in liquids.[1,2] Techniques such as two-dimensional Raman[3–7] and two- and three-dimensional infrared (IR) spectroscopes[8–13] are now being used to investigate the interactions between the inter- and intramolecular modes[14–22] as well as the dephasing mechanism of vibrational motions[23–26] that relate to the homogeneity versus inhomogeneity of liquids. The homogeneous broadening or vibrational dephasing of signals arise from the solvent motion occurring on time scales comparable to the time scales of vibration, while the inhomogeneous broadening is arising from the liquid features that change so slowly and look essentially static.[27,28] The anharmonic coupling between the inter- and intramolecular modes as well as dipole and induced dipole interactions also play an important role for energy and coherent relaxation processes in liquids.[29–32] The contributions to the signals from them can be distinguished as a difference of profiles or different spectral peaks in multidimensional spectroscopy, which is similar to the spin echo measurement for dephasing and the two-dimensional nuclear magnetic resonance measurement for the well-known coupling effects between spins. The advanced experiments such as multidimensional spectroscopies need to be guided by theoretical calculations and simulations, since a relationship between the molecular motion and signals is not simple for such complex systems as molecular liquids, and other nonlinear processes may overlap with the signal of interest due to the complexity of the experimental setups.

For analyzing the detail of experimental results, molecular dynamics (MD) simulations are helpful means since they can predict not only the line shape and intensities of the signals but also the role of molecular interactions through the capability of changing the interaction potentials. Previous simulations for two-dimensional (2D) IR spectroscopy have used the basic strategy to ascertain the importance of the structure change or vibrational dephasing by partitioning the role of the environment, as taken from the MD simulation in the form of the fluctuations of the vibrational energy states, then calculated the signals by employing the analytical expression of the third-order response function of infrared echo measurements.[33–41] This procedure works fairly well for cases where the modes to be observed and the solvent or environment modes are well separated.[21] This procedure

---

[a] Electronic mail: hasegawa@kuchem.kyoto-u.ac.jp.

does not work, however, if the target modes and the environment are strongly coupled or the target modes are not well defined due to the structure or conformal changes of molecules that are influenced by the bath. In addition, even in the well separated case, this procedure does not provide a legitimate description of bath effects for a long time period since the bath modes cause not only fluctuations in the energy levels but also energy dissipation which leads the system to thermal equilibrium as described through fluctuation-dissipation theorem.[21,26] The most rigorous way to calculate nonlinear signals of complex system is to perform full MD calculations to simulate response functions. From the full MD approach, the absolute magnitude of the response function in relation to other background signal may be deduced from this procedure, which is extremely useful to compare the predicted signals with the experimental results. Note that, although exact calculations must be based on quantum molecular dynamics simulation, the quantum effects usually play a minor role for vibrational spectroscopy in condensed phases other than the zero point oscillation of high-frequency intramolecular modes. Therefore, classical molecular dynamics simulations and, if necessary, with some quantum corrections may be accurate enough to simulate most of experimental data of the 2D IR spectroscopies.

While the molecular dynamics simulation techniques themselves are well established, the calculation of the nonlinear response functions from full MD simulations is not well explored. This is because nonlinear vibrational spectroscopy became experimentally possible recently and the calculation of nonlinear response functions is extremely difficult due to the high sensitivity of the stability matrix elements involved in the nonlinear response functions.[42–46] As was pointed out, while the conventional one-dimensional Raman and linear IR spectroscopies analyze the harmonicity of molecular motions, the multidimensional Raman and IR spectroscopies can detect nonharmonic motions of molecules by eliminating the harmonic contribution to the signals.[26] This feature of multidimensional spectroscopies also makes the simulation difficult since we cannot apply the normal mode analysis which assumes harmonic motions for inter- and intramolecular modes.

Three MD methods have been developed for 2D Raman spectroscopy. The first one is the equilibrium approach that computes, exactly or approximately, a nonlinear optical response function expressed in the multiple Poisson brackets of the equilibrium molecular trajectories.[42,44,47–51] The second method is the nonequilibrium MD (NEMD) approach that performs the 2D spectroscopy experiment on the computer.[52–55] In the NEMD approach, the Raman polarizability is directly calculated from NEMD trajectories under a pair of external laser pulses with different time sequences. The third method hybridizes the first and second methods to avoid the time-consuming calculations of the stability matrices which are inherent in the equilibrium method with using nonequilibrium trajectories for a single laser excitation.[56,57]

In this paper, we use the NEMD approach to calculate the signals of 2D and three-dimensional (3D) IR spectroscopies. To reduce the number of necessary NEND trajectories, we decompose the third-order response function into doorway and window parts.[58,59] While the conventional NEMD simulation utilizes the trajectories from the initial equilibrium state to the final state, our approach goes from the decomposed state to the final state (forward in time) for the window part and the decomposed state to the initial state (backward in time) for the doorway part. It is shown that the NEMD approach with the forward-backward trajectories sampling method enhances the efficiency of the numerical simulation for such multidimensional IR spectroscopy as three-pulse IR photon echo measurement. To demonstrate the accuracy and efficiency of the present approach, we have evaluated the signals of 2D and 3D IR vibrational spectroscopies for liquid hydrogen fluoride. The liquid HF forms the hydrogen bond network in a zigzag chain structure due to the strong hydrogen bond interactions and quadrupole moment of HF molecules.[60–65] Thus, the liquid HF exhibits unusually narrow inhomogeneous linewidth in contrast to liquid water[64–79] and is an interesting target even for demonstration. The one-dimensional character of the hydrogen bond network also makes the conceptualization of the spatial correlations simple.

This paper is organized as follows. In Sec. II, we explain our simulation method for the third-order IR response function. In Sec. III, we show the results of the simulations for liquid hydrogen fluoride. Section IV is devoted to concluding remarks.

II. SIMULATION METHODS

A. Doorway and window functions

Since the extension to N particle systems in three-dimensional space is straightforward, we start from a one-dimensional particle system described by the Hamiltonian $H(p,q)$, where p and q are the momentum and coordinate of the particle, respectively. In the third-order IR measurement, the system interacts with the three IR pump pulses $H_I = -\mu(q)\Sigma_{k=a,b,c}E_k(t)$, where $\mu(q)$ is the molecular dipole and $E_k(t)$ is the time envelopment of the kth pulse, and then the excited molecular dipole is detected by the probe pulse. If we consider the impulsive pump pulses, $E_a(t)=E_a\delta(t)$, $E_b(t) = E_b\delta(t-t_1)$, and $E_c(t)=E_c\delta(t-t_1-t_2)$, and probe the dipole at $t=t_1+t_2+t_3$, the third-order IR response is expressed in terms of the molecular dipole moments as[66]

$$R(t_3,t_2,t_1) = \frac{(i)^3}{\hbar^3}\langle[[[\hat{\mu}(t_1+t_2+t_3),\hat{\mu}(t_1+t_2)],\hat{\mu}(t_1)],\hat{\mu}(0)]\rangle, \tag{2.1}$$

where $\hat{\mu}(t)$ is the Heisenberg operator of the dipole moment $\mu(\hat{q})$. The molecular states in the response functions are expressed in the Liouville space brackets $|q,q^\dagger\rangle\rangle \equiv |q\rangle\langle q^\dagger|$ and $\langle\langle q,q^\dagger|\hat{\rho} \equiv \langle q|\hat{\rho}|q^\dagger\rangle$ for any density operator $\hat{\rho}$. The initial equilibrium distribution and the trace operation are then expressed respectively as $e^{-\beta\hat{H}}/Z = |\rho^{\mathrm{eq}}\rangle\rangle$ and $\int d\mathbf{\Gamma}_{t_R}\langle\langle\mathbf{\Gamma}| \equiv \int\int dq dq^\dagger \delta(q-q^\dagger)\langle\langle q,q^\dagger|$, where $\beta = 1/k_BT$ and Z is the partition function. We denote the commutation operator of the Hamiltonian (the quantum Liouvillian) and the dipole by $e^{-i\hat{L}t}\hat{A} \equiv e^{-i\hat{H}t/\hbar}\hat{A}e^{i\hat{H}t/\hbar}$ with $i\hat{L}\hat{A} \equiv i[\hat{H},\hat{A}]/\hbar$ and $\hat{\mu}^\times\hat{A} \equiv \hat{\mu}\hat{A}$

$-\hat{A}\hat{\mu}$ for a right-hand side operator $\hat{A}$. The response functions can be rewritten as

$$R(t_3,t_2,t_1)=\frac{(i)^3}{\hbar^3}\int d\mathbf{\Gamma}_{t_R}\langle\langle\mathbf{\Gamma}|\hat{\mu}e^{-i\hat{L}t_3}\hat{\mu}^{\times}e^{-i\hat{L}t_2}\hat{\mu}^{\times}e^{-i\hat{L}t_1}\hat{\mu}^{\times}|\rho^{\mathrm{eq}}\rangle\rangle. \tag{2.2}$$

By inserting the completeness relation $1=\int\int dq'dq'^{\dagger}|q',q'^{\dagger}\rangle\rangle\langle\langle q',q'^{\dagger}|\equiv\int d\mathbf{\Gamma}'|\mathbf{\Gamma}'\rangle\rangle\langle\langle\mathbf{\Gamma}'|$, we can decompose the response functions into the doorway and window functions as[58,59]

$$R(t_3,t_2,t_1)=\int d\mathbf{\Gamma}'W_{cd}(t_2+t_3;\mathbf{\Gamma}')D_{ab}(\mathbf{\Gamma}';t_1). \tag{2.3}$$

The window function is defined by

$$W_{cd}(t_2+t_3;\mathbf{\Gamma}')\equiv\frac{i}{\hbar}\int d\mathbf{\Gamma}_{t_R}\langle\langle\mathbf{\Gamma}|\hat{\mu}e^{-i\hat{L}t_3}\hat{\mu}^{\times}e^{-i\hat{L}t_2}|\mathbf{\Gamma}'\rangle\rangle, \tag{2.4}$$

and is interpreted as the expectation value of $\hat{\mu}$ with the density operator $\hat{\rho}_c(t_2+t_3)=\exp[-i\hat{L}t_3]\hat{\mu}^{\times}\exp[-i\hat{L}t_2]|\mathbf{\Gamma}'\rangle\rangle$ that was initially in the uniform (flat) distribution $|\mathbf{\Gamma}'\rangle\rangle$ then interacted with the third-pump pulse $\hat{\mu}^{\times}$ between the time evolutions $\exp[-i\hat{L}t_2]$ and $\exp[-i\hat{L}t_3]$. The doorway function is defined by

$$D_{ab}(\mathbf{\Gamma}';t_1)\equiv\frac{(i)^2}{\hbar^2}\langle\langle\mathbf{\Gamma}'|\hat{\mu}^{\times}e^{-i\hat{L}t_1}\hat{\mu}^{\times}|\rho^{\mathrm{eq}}\rangle\rangle. \tag{2.5}$$

This is the probability distribution of the uniform distribution $\langle\langle\mathbf{\Gamma}'|$ for the density operator $\hat{\rho}_{ab}(t_1)=\hat{\mu}^{\times}\exp[-i\hat{L}t_1]\hat{\mu}^{\times}|\rho^{\mathrm{eq}}\rangle\rangle$. This operator corresponds to the expectation value of $\hat{\mu}^{\times}$ for density operator at time t_1 started from the initial state with the first pump excitation $\hat{\mu}^{\times}|\rho^{\mathrm{eq}}\rangle\rangle$.

In the Wigner representation, the distribution function is expressed as[67,68]

$$P(p,q)=\frac{1}{2\pi\hbar}\int_{-\infty}^{\infty}dx e^{ip\cdot x/\hbar}\left\langle\left\langle q-\frac{x}{2},q+\frac{x}{2}|\rho\right\rangle\right\rangle. \tag{2.6}$$

The completeness relation is now given by $1=\int\int dp'dq'|p',q'\rangle\rangle\langle\langle p',q'|$. Then, the doorway and window functions are, respectively, rewritten as

$$\begin{aligned}W_{cd}(t_2+t_3;p',q')\equiv\int\int dpdq\mu(q)\exp[-L_W(p',q')t_3]\\ \times\mu_W^{\times}(q')\exp[-L_W(p',q')t_2]\\ \times\delta(p-p')\delta(q-q')\end{aligned} \tag{2.7}$$

and

$$\begin{aligned}D_{ab}(p',q';t_1)\equiv\int\int dp_0dq_0\delta(p_0-p')\delta(q_0-q')\\ \times\hat{\mu}_W^{\times}(q_0)\exp[-L_W(p_0,q_0)t_1]\\ \times\hat{\mu}_W^{\times}(q_0)P^{\mathrm{eq}}(p_0,q_0),\end{aligned} \tag{2.8}$$

where $-L_W(p,q)$ and $\hat{\mu}_W^{\times}(q)$ are the quantum Liouvillian and the dipole operator $i\hat{\mu}^{\times}/\hbar$ in the Wigner representation,[26] respectively, and $P^{\mathrm{eq}}(p_0,q_0)=\langle\langle p_0,q_0|\rho^{\mathrm{eq}}\rangle\rangle=e^{-\beta H(p_0,q_0)}/Z$.

To obtain the above expression, we inserted the completeness relation right after the second pump interaction. We can break the theoretical description at arbitrary point during the course of the time evolution by assuming the laser fields do not overlap at the assigned point, and rigorously recast the response function in terms of the two decomposed functions.[59] For the 2D IR case, it is convenient to decompose the response function into the doorway and window functions before the second pump excitation as

$$\begin{aligned}W_{bcd}(t_2+t_3;p',q')\equiv\int\int dpdq\mu(q)\exp[-L_W(p',q')t_3]\\ \times\mu_W^{\times}(q')\exp[-L_W(p',q')t_2]\\ \times\hat{\mu}_W^{\times}(q')\delta(p-p')\delta(q-q')\end{aligned} \tag{2.9}$$

and

$$\begin{aligned}D_a(p',q';t_1)\equiv\int\int dp_0dq_0\delta(p_0-p')\delta(q_0-q')\\ \times\exp[-L_W(p',q')t_1]\hat{\mu}_W^{\times}(q_0)P^{\mathrm{eq}}(p_0,q_0).\end{aligned} \tag{2.10}$$

In both cases, the response function is calculated by integrating over p' and q' as

$$R(t_3,t_2,t_1)=\int dp'dq'W_{cd}(t_2+t_3;p',q')D_{ab}(p',q';t_1) \tag{2.11}$$

or

$$R(t_3,t_2,t_1)=\int dp'dq'W_{bcd}(t_2+t_3;p',q')D_a(p',q';t_1). \tag{2.12}$$

Either in the quantum or classical case, the above expression indicates that the response function can be obtained from the separately calculated doorway and window functions for any p' and q'. Expressions for N particles system can be obtained by replacing $(p,q)\rightarrow(\mathbf{p},\mathbf{q})\equiv(p_1^{(x)},p_1^{(y)},\ldots,p_N^{(z)},q_1^{(x)},q_1^{(y)},\ldots,q_N^{(z)})$, $\hat{\mu}_W^{\times}(q)\rightarrow\hat{\mu}_W^{\times}(\mathbf{q})\delta(p-p')\delta(q-q')\rightarrow\delta(\mathbf{p}-\mathbf{p})\delta(\mathbf{q}-\mathbf{q}')\equiv\Pi_{j=1}^{N}\Pi_{a=x,y,z}\delta(p_j^{(a)}-p_j'^{(a)})\delta(q_j^{(a)}-q_j'^{(a)})$, $\int\int dpdq\rightarrow\int\int d\mathbf{p}d\mathbf{q}\equiv\Pi_{j=1}^{N}\Pi_{a=x,y,z}\int\int dp_j^{(a)}dq_j^{(a)}$, etc. The quantum and classical Liouvillians are given by

$$\begin{aligned}-L_W(\mathbf{p},\mathbf{q})=-\sum_{j=1}^{N}\sum_{a=x,y,z}\Bigg\{p_j^{(a)}\frac{\partial}{\partial q_j^{(a)}}\\ -\frac{1}{i\hbar}\sum_{k\neq j}\Bigg[U_{jk}\left(q_j^{(x)}-\frac{\hbar}{2i}\frac{\partial}{\partial p_j^{(a)}},\mathbf{q}_k\right)\\ -U_{jk}\left(q_j^{(a)}+\frac{\hbar}{2i}\frac{\partial}{\partial p_j^{(a)}},\mathbf{q}_k\right)\Bigg]\Bigg\}\end{aligned} \tag{2.13}$$

and

$$-L_{\mathrm{cl}}(\mathbf{p},\mathbf{q}) = -\sum_{j=1}^{N}\sum_{a=x,y,z}\left(p_j^{(a)}\frac{\partial}{\partial q_j^{(a)}} + \sum_{k\neq j}\frac{\partial U_{jk}(q_j^{(a)},\mathbf{q}_k)}{\partial q_j^{(a)}}\frac{\partial}{\partial p_j^{(a)}}\right), \qquad (2.14)$$

respectively, where $U_{jk}(\mathbf{q}_j,\mathbf{q}_k)$ is the interaction potential between the jth and kth particles. In this paper, we employ the classical Liouvillian to calculate the response function by means of MD simulations.

B. Nonequilibrium molecular dynamics simulation

We use the nonequilibrium (finite field) simulation approach to evaluate the doorway and window functions. The nonequilibrium approach allows us to calculate the physical observable from nonequilibrium simulations for different pulse configurations and sequences.[52,53]

In order to evaluate $W_{cd}(t;p',q')$, conventional finite field approaches utilize the unperturbed and perturbed Hamiltonians, H and $H_c(\tau)=H-E_c\mu(q)\delta(\tau-t_1-t_2)$, respectively. Instead, we have employed the inverted force method,[54] which considers $H_c(\tau)$ and the perturbed Hamiltonian with the opposite sign $H_{\bar{c}}(\tau)=H+E_c\mu(q)\delta(\tau-t_1-t_2)$. Using $H_{\bar{c}}(\tau)$ instead of H, we can efficiently eliminate the higher order contribution of the perturbation from the expectation values. We denote the Liouvillian for $H_c(\tau)$ and $H_{\bar{c}}(\tau)$ by $L_{\mathrm{cl}}^{c}(p',q';\tau)$ and $L_{\mathrm{cl}}^{\bar{c}}(p',q';\tau)$. The corresponding distribution functions are expressed as $P^c(p,q;p',q';t)=\exp[-\int_{t_1}^{t}d\tau L_{\mathrm{cl}}^{c}(p',q')]\delta(p-p')\delta(q-q')$ and $P^{\bar{c}}(p,q;p',q';t)=\exp[-\int_{t_1}^{t}d\tau L_{\mathrm{cl}}^{\bar{c}}(p',q';\tau)]\delta(p-p')\delta(q-q')$, respectively.

By treating the pump excitation E_c perturbatively, we can express the window function as

$$\begin{aligned} W_{cd}(t;p',q') &\approx \frac{1}{2E_c\Delta t}\int\int dp\,dq\,\mu(q)[P^c(p,q;p',q';t) \\ &\quad - P^{\bar{c}}(p,q;p',q';t)] \\ &\equiv \frac{1}{2E_c\Delta t}[\mu_c(p',q';t)-\mu_{\bar{c}}(p',q';t)], \end{aligned} \qquad (2.15)$$

where $t=t_2+t_3$ and $\mu_c(p',q';t)$ and $\mu_{\bar{c}}(p',q';t)$ mean the expectation values of the dipole for the perturbation $\mp E_c\mu(q)\delta(\tau-t_1-t_2)$. Since the even order contribution of the perturbation will be cancel out by adding $\mu_c(p',q';t)$ and $\mu_{\bar{c}}(p',q';t)$, the inverted method is quite efficient at calculating the third-order response functions.

C. Forward and backward propagations

Equations (2.7)–(2.12) indicate that the response function can be obtained from the separately calculated doorway and window functions for any $\mathbf{p}'$ and $\mathbf{q}'$. First, we consider $W_{cd}(t_2+t_3;\mathbf{p}',\mathbf{q}')$ and $D_{ab}(\mathbf{p}',\mathbf{q}';t_1)$, which are both in the second order of the dipole interactions. As explained above, $W_{cd}(t_2+t_3;\mathbf{p}',\mathbf{q}')$ is evaluated by the NEMD simulation from two nonequilibrium trajectories in phase space that start from initial values $\mathbf{p}'$ and $\mathbf{q}'$ in a uniform distribution and evolve forward in time for the perturbed Hamiltonians $H_c(\tau)$ and $H_{\bar{c}}(\tau)$. Accordingly, the doorway function $D_{ab}(\mathbf{p}',\mathbf{q}';t_1)$ is calculated from the nonequilibrium trajectories that start with initial values $\mathbf{p}_0$ and $\mathbf{q}_0$ in the equilibrium distribution and propagate forward in time for the Hamiltonians $H_b(\tau)=H-E_b\mu(\mathbf{q})\delta(\tau-t_1)$ and $H_{\bar{b}}(\tau)=H+E_b\mu(\mathbf{q})\delta(\tau-t_1)$ after operating the first pump excitation denoted by $i\hat{\mu}_W^{\times}(\mathbf{q})/\hbar$. Alternatively, we can evaluate the doorway function using the trajectories corresponding to the backward propagation in time. This can be done without considering the phase-space compression factor since we do not have any dissipation processes and the system dynamics is time reversible.[59,69] We rewrite Eq. (2.8) as

$$\begin{aligned} D_{ab}(\mathbf{p}',\mathbf{q}';t) \equiv \int\int d\mathbf{p}_0 d\mathbf{q}_0 P^{\mathrm{eq}}(\mathbf{p}_0,\mathbf{q}_0) \\ \times\hat{\mu}_W^{\times}(\mathbf{q}')\exp\left[-\int_{t_1}^{0}d\tau L_W(\mathbf{p}',\mathbf{q}';\tau)\right] \\ \times\hat{\mu}_W^{\times}(\mathbf{q}')\delta(\mathbf{p}_0-\mathbf{p}')\delta(\mathbf{q}_0-\mathbf{q}'). \end{aligned} \qquad (2.16)$$

The initial state of the backward trajectories $\mathbf{p}'$ and $\mathbf{q}'$ are in the uniform distribution. After operating the second pulse $i\hat{\mu}_W^{\times}(\mathbf{q})/\hbar$ to the initial state, we calculate the equilibrium and nonequilibrium trajectories from time t_1 to 0 for the Hamiltonians $H_{\bar{a}}(\tau)=H+E_a\mu(\mathbf{q})\delta(\tau)$ and $H_a(\tau)=H-E_a\mu(\mathbf{q})\delta(\tau)$ backward in time. The final state, which is the initial equilibrium state in the forward case, is defined by integration over $\mathbf{p}_0$ and $\mathbf{q}_0$ with the weight function $P^{\mathrm{eq}}(\mathbf{p}_0,\mathbf{q}_0)$.

As Eq. (2.11) indicates, we need to generate trajectories from a sampling point in the uniform distribution of $(\mathbf{p}',\mathbf{q}')$. In practice, however, we do not have to generate points of $(\mathbf{p}',\mathbf{q}')$ that are far from the equilibrium distribution $P^{\mathrm{eq}}(\mathbf{p}',\mathbf{q}')$. This is because the trajectories from those points give very small contributions to $D_{ab}(\mathbf{p}',\mathbf{q}';t_1)$ due to the factor $P^{\mathrm{eq}}(\mathbf{p}'(-t_1),\mathbf{q}'(-t_1))$, where $(\mathbf{p}'(0),\mathbf{q}'(0))\equiv(\mathbf{p}',\mathbf{q}')$ and $(\mathbf{p}'(-t_1),\mathbf{q}'(-t_1))$ are the backward trajectories from $t=0$ to $t=-t_1$ for the perturbed Hamiltonians $H_a(\tau)$ and $H_{\bar{a}}(\tau)$ with the second pump excitation. Thus, instead of using uniform distribution for $(\mathbf{p}',\mathbf{q}')$, we can generate the trajectories from the sampling points in the equilibrium distribution $P^{\mathrm{eq}}(\mathbf{p}',\mathbf{q}')$ and calibrate the weight of probability by multiplying $\exp[\beta E(\mathbf{p}',\mathbf{q}')]$, where $E(\mathbf{p}',\mathbf{q}')$ is the total energy of molecules for the configuration $(\mathbf{p}',\mathbf{q}')$. In this scheme, Eq. (2.11) is rewritten as

$$\begin{aligned} R(t_3,t_2,t_1) = \int d\mathbf{p}'d\mathbf{q}'\,W_{bcd}(t_2+t_3;\mathbf{p}',\mathbf{q}')P^{\mathrm{eq}}(\mathbf{p}',\mathbf{q}') \\ \times D_a'(\mathbf{p}',\mathbf{q}';t_1), \end{aligned} \qquad (2.17)$$

where

$$D_a'(\mathbf{p}',\mathbf{q}';t_1) = e^{\beta E(\mathbf{p}',\mathbf{q}')}D_a(\mathbf{p}',\mathbf{q}';t_1). \qquad (2.18)$$

The classical doorway function for the canonical distribution is expressed as

$$D'_a(\mathbf{p}',\mathbf{q}';t_1) \approx \frac{1}{2E_a\Delta t}\left\{\frac{\exp[-\beta\Delta H^a(\mathbf{p}',\mathbf{q}';-t_1)]}{Z^a} - \frac{\exp[-\beta\Delta H^{\bar{a}}(\mathbf{p}',\mathbf{q}';-t_1)]}{Z^{\bar{a}}}\right\}, \tag{2.19}$$

where $\Delta H^a = H^a(\mathbf{p},\mathbf{q};-t_1) - H^0(\mathbf{p},\mathbf{q};0)$ is the work done to the molecular system by the first laser interaction, and Z^a and $Z^{\bar{a}}$ are the partition functions for $H^a(\mathbf{p},\mathbf{q};-t_1)$ and $H^{\bar{a}}(\mathbf{p},\mathbf{q};-t_1)$, respectively. Since we have the relation

$$\Delta H^a(\mathbf{p}',\mathbf{q}';-t_1) \approx \sum_i \frac{p_i(-t_1)}{m}\frac{\partial\mu(-t_1)}{\partial q_i^{(\alpha)}(-t_1)}E_a\Delta t = \dot{\mu}(-t_1)E_a\Delta t, \tag{2.20}$$

by expanding Eq. (2.19) in terms of laser interactions and by collecting the terms in the order of E_a, we can obtain the simple expression

$$D'_a(\mathbf{p}',\mathbf{q}';t_1) \approx -\frac{\beta}{2}\left\{\dot{\mu}(\mathbf{p}',\mathbf{q}';-t_1) - \frac{1}{Z}\int d\mathbf{p}d\mathbf{q} \times\exp[-\beta H^0(\mathbf{p},\mathbf{q};0)]\dot{\mu}(\mathbf{p},\mathbf{q};-t_1)\right\}, \tag{2.21}$$

which enables us to calculate the doorway function from equilibrium trajectories. This expression is convenient to calculate the two-dimensional third-order response function. The window function in Eq. (2.17) is expressed as

$$W_{bcd}(t_2+t_3;\mathbf{p}',\mathbf{q}') \approx \frac{1}{4E_bE_c(\Delta t)^2}\{\mu_{bc}(\mathbf{p}',\mathbf{q}';t_2+t_3) + \mu_{\bar{b}\bar{c}}(\mathbf{p}',\mathbf{q}';t_2+t_3) - \mu_{\bar{b}c}(\mathbf{p}',\mathbf{q}';t_2+t_3) - \mu_{b\bar{c}}(\mathbf{p}',\mathbf{q}';t_2+t_3)\}, \tag{2.22}$$

and the response function is evaluated as

$$R(t_3,t_2,t_1) = \frac{-\beta}{4E_bE_c(\Delta t)^2}\langle\{\mu_{bc}(t_2+t_3) + \mu_{\bar{b}\bar{c}}(t_2+t_3) - \mu_{\bar{b}c}(t_2+t_3) - \mu_{b\bar{c}}(t_2+t_3)\} \times\Delta\dot{\mu}(-t_1)\rangle_{NVT,\mathrm{adiabatic}}, \tag{2.23}$$

where $\langle A(t)\rangle_{NVT,\mathrm{adiabatic}}$ denotes the average value of the function $A(t)$ in initially the canonical and then the adiabatically evolving ensemble and $\Delta\dot{\mu}(-t_1) = \dot{\mu}(-t_1) - \langle\dot{\mu}(-t_1)\rangle_{NVT,\mathrm{adiabatic}}$. This expression is equivalent to the equilibrium and nonequilibrium hybrid MD method developed to simulate fifth-order two-dimensional Raman spectroscopy.[56]

Alternatively, we can rewrite Eq. (2.11) as

$$R(t_3,t_2,t_1) = \int d\mathbf{p}'d\mathbf{q}'W_{cd}(t_2+t_3;\mathbf{p}',\mathbf{q}') \times P^{\mathrm{eq}}(\mathbf{p}',\mathbf{q}')D'_{ab}(\mathbf{p}',\mathbf{q}';t_1), \tag{2.24}$$

where $D'_{ab}(\mathbf{p}',\mathbf{q}';t_1) = e^{\beta E(\mathbf{p}',\mathbf{q}')}D_{ab}(\mathbf{p}',\mathbf{q}';t_1)$. The classical doorway function in Eq. (2.24) is written as

$$D'_{ab}(\mathbf{p}',\mathbf{q}';t_1) \approx \frac{1}{4E_aE_b(\Delta t)^2}\left\{\frac{\exp[-\beta\Delta H^{ab}(\mathbf{p}',\mathbf{q}',-t_1)]}{Z^{ab}} + \frac{\exp[-\beta\Delta H^{\bar{a}\bar{b}}(\mathbf{p}',\mathbf{q}',-t_1)]}{Z^{\bar{a}\bar{b}}} - \frac{\exp[-\beta\Delta H^{a\bar{b}}(\mathbf{p}',\mathbf{q}',-t_1)]}{Z^{a\bar{b}}} - \frac{\exp[-\beta\Delta H^{\bar{a}b}(\mathbf{p}',\mathbf{q}',-t_1)]}{Z^{\bar{a}b}}\right\}, \tag{2.25}$$

where $\Delta H^{ab} = H^{ab}(\mathbf{p},\mathbf{q};-t_1) - H^0(\mathbf{p},\mathbf{q};0)$ is the work done to the molecular system by the first and second laser interactions and Z^{ab} is the partition function for $H^{ab}(\mathbf{p}',\mathbf{q}',-t_1)$. Using the relation

$$\Delta H^{ab}(-t_1) \approx \sum_i \frac{p_i(0)}{m}\frac{\partial\mu(0)}{\partial q_i^{(\alpha)}(0)}E_b\Delta t + \sum_i \frac{p_{i,b}(-t_1)}{m}\frac{\partial\mu_b(-t_1)}{\partial q_{i,b}^{(\alpha)}(-t_1)}E_a\Delta t = \dot{\mu}(0)E_b\Delta t + \dot{\mu}_b(-t_1)E_a\Delta t, \tag{2.26}$$

and expanding Eq. (2.25) to collect the terms in the order of E_aE_b, we obtain

$$D'_{ab}(\mathbf{p}',\mathbf{q}';t_1) \approx \frac{1}{Z}\left\{\frac{-\beta}{2E_b\Delta t}(\dot{\mu}_b(\mathbf{p}',\mathbf{q}';-t_1) - \dot{\mu}_{\bar{b}}(\mathbf{p}',\mathbf{q}';-t_1)) + \beta^2\dot{\mu}(\mathbf{p}',\mathbf{q}';-t_1)\dot{\mu}(\mathbf{p}',\mathbf{q}';0)\right\} - \frac{1}{Z^2}\int d\mathbf{p}d\mathbf{q}\left\{\frac{-\beta}{2E_b\Delta t}(\dot{\mu}_b(\mathbf{p},\mathbf{q};-t_1) - \dot{\mu}_{\bar{b}}(\mathbf{p},\mathbf{q};-t_1)) + \beta^2\dot{\mu}(\mathbf{p},\mathbf{q};-t_1) \times\dot{\mu}(\mathbf{p},\mathbf{q};0)\right\}\exp[-\beta H^0(\mathbf{p},\mathbf{q};0)]. \tag{2.27}$$

The corresponding classical window function is given by Eq. (2.15). Then, the response function is expressed as

$$R(t_3,t_2,t_1) = \left\langle \frac{1}{2E_c\Delta t}[\mu_c(t_2+t_3) - \mu_{\bar{c}}(t_2+t_3)]\left\{\frac{-\beta}{2E_b\Delta t}[\dot{\mu}_b(-t_1) - \dot{\mu}_{\bar{b}}(-t_1)] + \beta^2\dot{\mu}(-t_1)\dot{\mu}(0)\right\}\right\rangle_{NVT,\mathrm{adiabatic}} - \left\langle \frac{1}{2E_c\Delta t}[\mu_c(t_2+t_3) - \mu_{\bar{c}}(t_2+t_3)]\right\rangle_{NVT,\mathrm{adiabatic}}\left\langle \frac{-\beta}{2E_b\Delta t}[\dot{\mu}_b(-t_1) - \dot{\mu}_{\bar{b}}(-t_1)] + \beta^2\dot{\mu}(-t_1)\dot{\mu}(0)\right\rangle_{NVT,\mathrm{adiabatic}}. \tag{2.28}$$

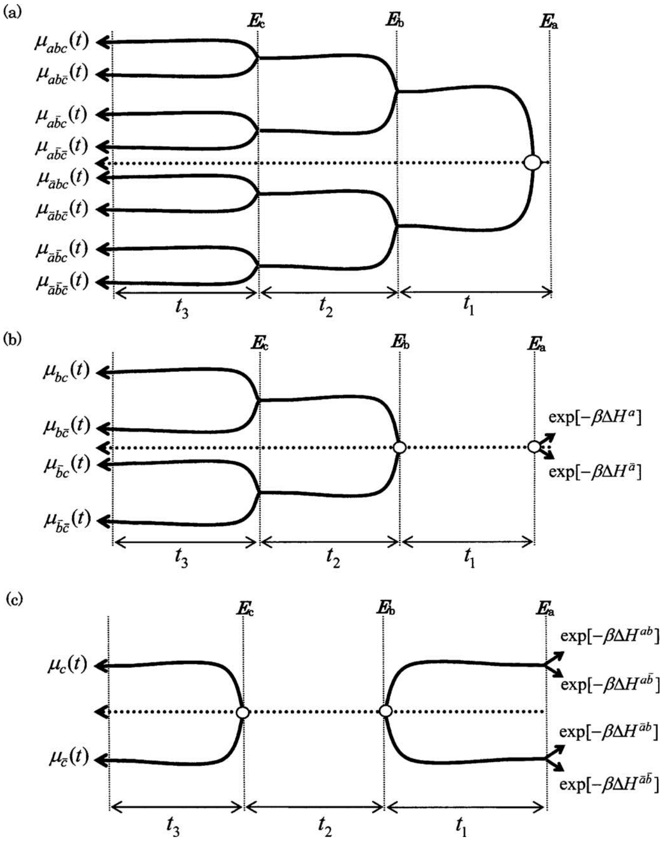

FIG. 1. The simulation processes are illustrated. The thick lines correspond to adiabatic NEMD trajectories. The dotted lines correspond to equilibrium *NVE* (constant energy) trajectories. White circles are the initial configurations of the adiabatic NEMD calculations. The dotted lines or equilibrium trajectories should be generated from canonical ensembles. The exponential terms can be calculated by the time derivative of the dipole moment [Eqs. (2.22) and (2.27)]. (a) Conventional NEMD method. Eight NEMD trajectories are used to extract the third-order response from the total response. (b) The simulation process using Eq. (2.22). Four NEMD trajectories and one equilibrium trajectory are employed. (c) The simulation process using Eq. (2.27). Two NEMD trajectories, two backward NEMD trajectories, and one equilibrium trajectory are used. The trajectory in the t_2 period corresponds to the equilibrium one.

This expression is convenient to calculate the 3D third-order response function. The number of necessary nonequilibrium simulations for the third-order response function depends on the calculation schemes. The simulation processes for the conventional NEMD method and the developed two schemes are schematically illustrated in Fig. 1. Notice that the second term in Eq. (2.28) will vanish if we sample the whole phase points because this term arises from the difference between the partition functions involved in Eq. (2.28). To obtain accurate signals from the finite number of the phase points, we need to include this term.

In the next section, we examine the accuracy and efficiency of our approach by calculating the 2D and 3D signals for liquid hydrogen fluoride.

III. TWO-AND THREE-DIMENSIONAL IR SIGNALS OF HYDROGEN FLUORIDE LIQUID

A. Computational details

To simulate 2D and 3D IR signals for liquid hydrogen fluoride, we used the FF(64,0.78) intermolecular potential expressed in the Chebyshev expansion form.[64] The Ewald method was used for the long range Coulomb interactions. The simulation was carried out with 64 HF molecules. The total dipole moment was calculated by the first-order dipole-induced-dipole approximation and the dipole moment and the molecular polarizability were taken from experimental values.[70–73] The simulation box was a 1.29 nm^3 and the short range forces were cut off at the half length of the simulation box. The equations of motion were solved by the velocity-Verlet integrator of rigid bodies[74,75] with the time step of 0.1 fs for canonical (*NVT*) calculations and 2 fs for microcanonical (*NVE*) calculations. The Nose-Hoover chain with 20 thermostats was used to generate the *NVT* ensemble. The *NVT* simulations were performed at 273 K. We set $E\Delta t = 1.0\times 10^{-5}$ V m^{-1} s in the NEMD calculations. The laser fields are applied during very short time step of $\Delta t = 1.0 \times 10^{-40}$ fs to obtain the impulsive responses. We first made 3×10^4 temporary configurations from a *NVT* trajectory at 4 ps intervals in order to prepare the *NVT* ensemble. We then took fragments of the 4 ps *NVE* trajectory from the temporary configurations after 4 ps equilibrations. The initial configuration of the NEMD calculations was sampled at 4 fs intervals from each fragment of the trajectories. Then, the signals were calculated by averaging over the 3×10^7 initial configurations.

B. The accuracy and efficiency of the simulation

First, we compared the accuracy and efficiency of third-order 2D IR signals for fixed $t_2=0$ calculated from the two

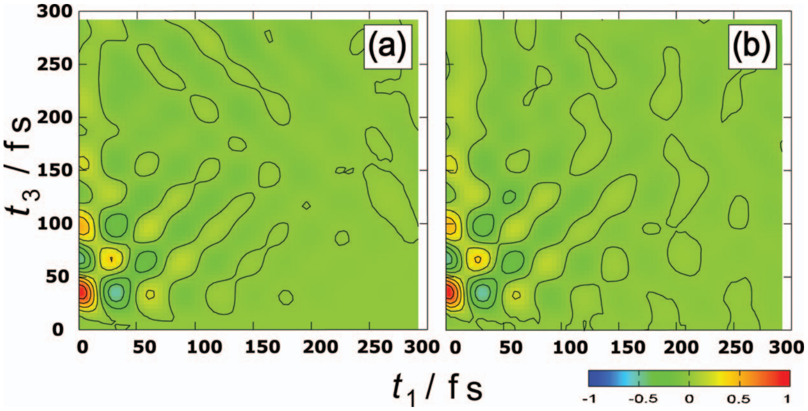

FIG. 2. (Color) The time domain third-order response function $R_{zzzz}(t_1, 0, t_3)$ for liquid HF at $t_2=0$ fs. Panels (a) and (b) are calculated from Eqs. (2.22) and (2.27), respectively. The signal strengths are normalized by the peak strength of the signal in panel (a).

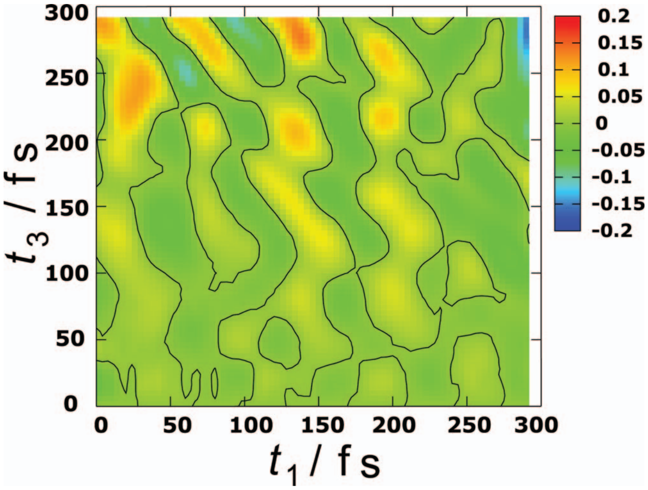

FIG. 3. (Color) The difference in the third-order response functions calculated from Eqs. (2.22) and (2.27).

different schemes of the doorway and window decompositions. The first scheme is expressed as Eq. (2.23) and is based on the decomposition before the second pump excitation, while the second scheme is expressed as Eq. (2.28) and is decomposed after the second pump excitation. We calculated the third-order response functions for all parallel polarization $R_{zzzz}(t_1,0,t_3)$ based on the two schemes. The results of the first and second schemes are given in Figs. 2(a) and 2(b), respectively. The signal profiles and strength are almost the same. However, there are some disagreements in the region $t_3 > 150$ fs, which is depicted in Fig. 3 as the difference between the two profiles. This is because the signal from the first scheme converges slower than that from the second scheme in the region of $t_3 < 50$ fs. In the first scheme, the window function is defined by the second-order difference of the dipole moment, so that the true signal is very weak compared to the thermal fluctuation noise in the region of $t_3 > 150$ fs and the signal converges slower in the first scheme than the second scheme in this region.

The second scheme allows us to calculate the 3D signals for different t_2 much faster than the fast scheme. This is because the second scheme uses equilibrium trajectories in the t_2 period and we can calculate the third order responses for different t_2 by choosing pairs of initial configurations on one *NVE* fragment for the doorway and window functions. In the first scheme, however, we need to repeat the NEMD calculation for each t_2 to have 3D signals as a function of t_1, t_2, and t_3.

C. The time-domain and frequency-domain signals

Figures 4(a)–4(f) illustrate the time-domain 2D IR signals for liquids HF with all parallel polarizations. The oscillations of the period of 60 fs are induced by the intermolecular vibrational motions of the hydrogen bonds. The signal profile in Fig. 4(a) resembles the 2D IR signal calculated from Gaussian-Markovian Fokker-Planck equation with a linear-linear (LL) and square-nonlinear (SL) system-bath couplings.[26,28,76,77] The conventional Brownian oscillator model considers the LL interaction which describes the damping and thermal activation processes of the Langevin dynamics. The SL interaction changes the curvature of the system potential,[78] which in turn causes the vibrational dephasing process. Analogous to the case of electronically resonant spectroscopy, LL interactions induce the longitudinal (T_1) and transverse (T_2) relaxations, whereas SL interactions induce similar effects as the inhomogeneous broadening.[26] Figure 4(a) exhibits similar profiles, as shown in Fig. 15(v) of Ref. 26, which corresponds to a slow modulation (inhomogeneous) case of an anharmonic Brownian oscillator system. The phase difference of the signals in Fig. 4(a) and Fig. 15(v) in Ref. 26 may be attributed to the nonlinear coordinate dependence of the dipole moment of liquid hydrogen fluoride. The echo like profile along $t_1 = t_3$ vanishes around $t_2 = 200$ fs, which is the same order as the noise correlation time estimated from the results of the LL+SL model [Fig. 15(v) in Ref. 26] as $1/\gamma = 1/(0.1\omega_0) \approx 500$ fs.

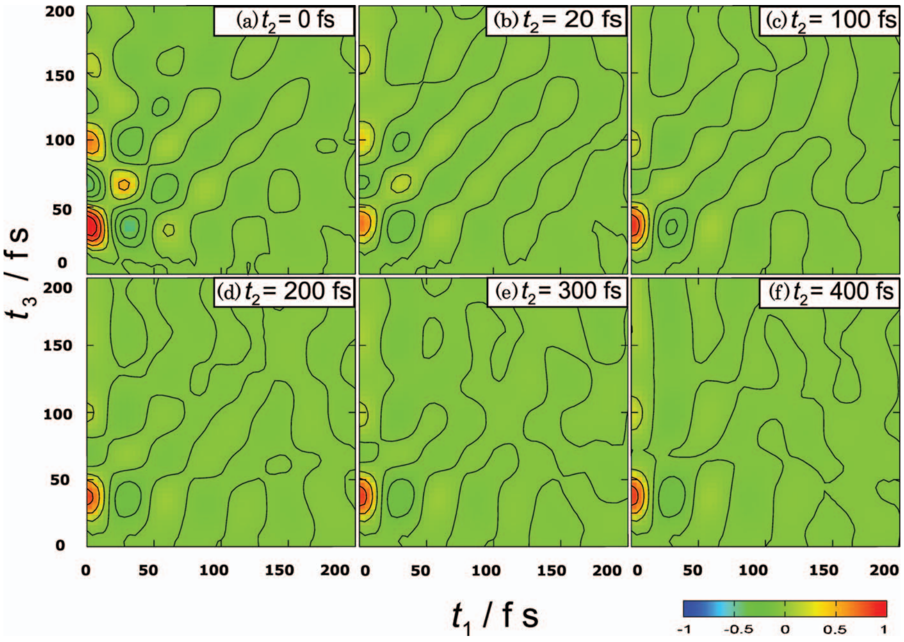

FIG. 4. (Color) The time domain third-order response functions $R_{zzzz}(t_1,t_2,t_3)$ at (a) $t_2 = 0$ fs, (b) $t_2 = 20$ fs, (c) $t_2 = 100$ fs, (d) $t_2 = 200$ fs, (e) $t_2 = 300$ fs, and (f) $t_2 = 400$ fs calculated from Eq. (2.27). The signal strengths are normalized by peak strength of the original signal shown in (a).

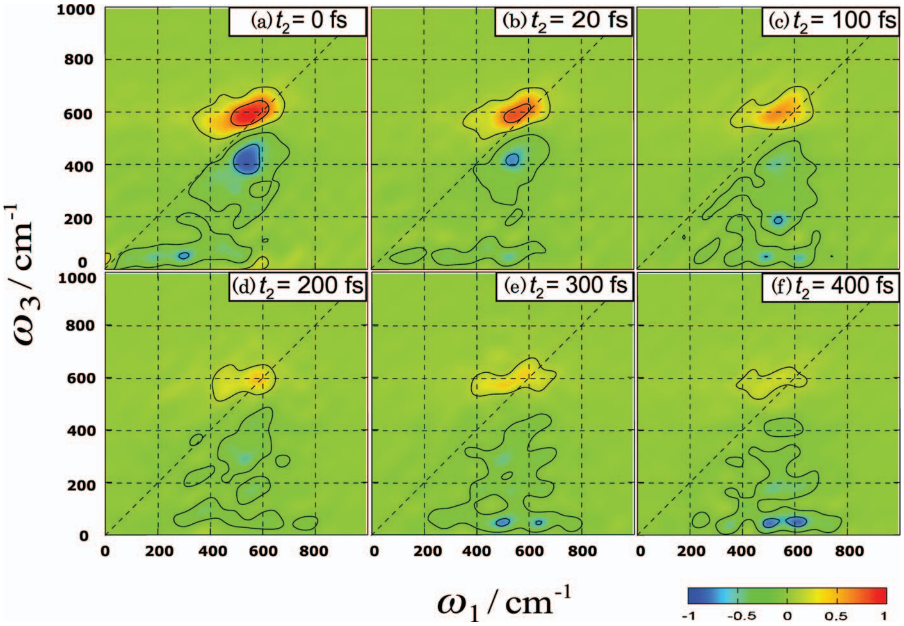

FIG. 5. (Color) The correlation spectra of liquid HF at (a) $t_2=0$ fs, (b) $t_2=20$ fs, (c) $t_2=100$ fs, (d) $t_2=200$ fs, (e) $t_2=300$ fs, and (f) $t_2=400$ fs.

We next present the frequency domain correlation spectra for different t_2 to discuss the role of dephasing and anharmonicity on the vibrational modes.[10,21] We calculated the correlation spectra in the following procedure. First we have performed a 3D Fourier transformation of the signal with all parallel polarization in t_1, t_2, and t_3. We then took the signal only in the range of $\omega_2 < 200$ cm^{-1} and reconverted it into a time domain in t_2. The correlation spectra was obtained by adding the imaginary part of $(\omega_1,\omega_3)=(+,+)$ quadrant and $(\omega_1,\omega_3)=(-,+)$ quadrant. Figures 5(a)–5(f) show the correlation spectra with the waiting time $t_2=0$, 20, 100, 200, 300, and 400 fs, respectively. In each figure, we see a positive peak around $(\omega_1,\omega_3)=(550,550)$ cm^{-1} corresponding to the vibrational coherence from the fundamental oscillation, and a negative peak around $(\omega_1,\omega_3)=(550,400)$ cm^{-1} corresponding to the vibrational coherence from an anharmonic oscillation. These peaks are induced by the vibrational motion of the hydrogen bonds network in the liquid HF. The width of the peak at $(\omega_1,\omega_3)=(550,550)$ is about 50 cm^{-1} and is much narrower than the inhomogeneous linewidth observed in liquid water.[79] This is due to the formation of the strong hydrogen bonds and one-dimensional character of HF molecule.[60–65] This narrow band feature is also supported by the recent neutron scattering experiment.[80]

As expected for intermolecular vibrational motions, a large anharmonicity (≈ 150 cm^{-1}) is observed. Since we neglected the intramolecular vibrational motion of HF, no energy transfer take place between the intermolecular and intramolecular motions. To have effects from intramolecular motions, one has to employ a multibody intramolecular potential instead of a simple harmonic potential.[65] In addition, since quantum effects may play some roles in the high frequency intramolecular vibrational mode, one has to involve a quantum correction in the simulations. These two challenging tasks are left for further studies.

IV. CONCLUSIONS

The present paper describes a methodology to efficiently calculate the signals of 2D and 3D third-order IR spectroscopies by means of the NEMD simulation. The key features of this approach are the doorway-window decomposition of the response function and the backward-forward sampling of the NEMD trajectories. The efficiency and accuracy of the simulation were tested to calculate 2D and 3D IR signals of liquid HF using two different schemes of the doorway-window decompositions. The scheme represented by Eq. (2.28) makes the calculation of 3D IR signals more efficient than the conventional NEMD method and the scheme represented by Eq. (2.23). Using the scheme represented by Eq. (2.28), we calculated the 3D signals for different t_2. The calculated signal exhibits vibrational dephasing within a correlation time of $\tau \approx 200$ fs, which may be described by an anharmonic Brownian oscillator model with linear-linear and square-liner system-bath couplings. The anharmonicity of intermolecular vibrational modes was also confirmed by the frequency domain correlation spectra. We presented the efficient algorithm to calculate the 3D IR signals for the intermolecular vibrational motions, without including the intramolecular contribution. The developments of the multibody intramolecular potential and the calculation strategy of the quantum corrections are necessary for further studies.

ACKNOWLEDGMENTS

The authors thank A. Ishizaki, S. Saito, T. Yagasaki, and R. J. D. Miller for their helpful discussions. Y.T. is thankful for the financial support from a Grant-in-Aid for Scientific Research B19350011 from the Japan Society for the Promotion of Science. T.H. is supported by the research fellowship of Global COE program, International Center for Integrated Research and Advanced Education in Material Science, Kyoto University, Japan. A part of the computations was performed at Research Center for Computational Science, Okazaki, Japan.

[1] Y. Tanimura and S. Mukamel, J. Chem. Phys. **99**, 9496 (1993).
[2] P. Hamm, M. Lim, and R. M. Hochstrasser, Phys. Rev. Lett. **81**, 5326 (1998).

[3] V. Astinov, K. J. Kubarych, C. J. Milne, and R. J. D. Miller, Chem. Phys. Lett. **327**, 3334 (2000).
[4] K. J. Kubarych, C. L. Milne, S. Lin, V. Astinov, and J. D. Miller, J. Chem. Phys. **116**, 2016 (2002).
[5] K. J. Kubarych, C. L. Milne, and R. J. D. Miller, Chem. Phys. Lett. **369**, 635 (2003).
[6] L. J. Kaufman, J. Heo, L. D. Ziegler, and G. R. Fleming, Phys. Rev. Lett. **88**, 207402 (2002).
[7] C. J. Milne, Y. L. Li, T. I. C. Jansen, L. Huang, and R. J. D. Miller, J. Phys. Chem. B **110**, 19867 (2006).
[8] P. Hamm, M. Lim, and R. M. Hochstrasser, J. Phys. Chem. B **102**, 6123 (1998).
[9] M. T. Zanni, S. Gnanakaran, J. Stenger, and R. M. Hochstrasser, J. Phys. Chem. B **105**, 6520 (2001).
[10] N. Demirdoeven, M. Khalil, and A. Tokmakoff, Phys. Rev. Lett. **89**, 237401 (2002).
[11] M. Khalil, N. Demirdoven, and A. Tokmakoff, J. Phys. Chem. A **107**, 5258 (2003).
[12] K. Ohta, H. Maekawa, S. Saito, and K. Tominaga, J. Phys. Chem. A **107**, 5643 (2003).
[13] M. Cho, Bull. Korean Chem. Soc. **27**, 1940 (2006).
[14] K. A. Merchant, W. G. Noid, R. Akiyama, I. J. Finkelstein, A. Goun, B. L. McClain, R. F. Loring, and M. D. Fayer, J. Am. Chem. Soc. **125**, 13804 (2003).
[15] N. Demirdoven, C. M. Cheatum, H. S. Chung, M. Khalil, J. Knoester, and A. Tokmakoff, J. Am. Chem. Soc. **126**, 7981 (2004).
[16] J. B. Asbury, T. Steinel, C. Stromberg, K. J. Gaffney, I. R. Piletic, A. Goun, and M. D. Fayer, Phys. Rev. Lett. **91**, 237402 (2003).
[17] J. B. Asbury, T. Steinel, and M. D. Fayer, J. Phys. Chem. B **108**, 6544 (2004).
[18] I. V. Rubtsov, K. Kumar, and R. M. Hochstrasser, Chem. Phys. Lett. **402**, 439 (2005).
[19] M. L. Cowan, B. D. Bruner, N. Huse, J. R. Dwyer, B. Chugh, E. T. J. Nibbering, T. Elsaesser, and R. J. D. Miller, Nature (London) **434**, 199 (2005).
[20] J. T. Fourkas, Adv. Chem. Phys. **117**, 235 (2001).
[21] A. Ishizaki and Y. Tanimura, J. Chem. Phys. **125**, 084501 (2006).
[22] A. Ishizaki and Y. Tanimura, J. Phys. Chem. A **111**, 9269 (2007).
[23] M. Cho, PhysChemComm **7**, 1 (2002).
[24] K. Ohta, H. Maekawa, S. Saito, and K. Tominaga, J. Phys. Chem. A **107**, 5643 (2003).
[25] J. B. Asbury, T. Steinel, C. Stromberg, S. A. Corcelli, C. P. Lawrence, J. L. Skinner, and M. D. Fayer, J. Phys. Chem. A **108**, 1107 (2004).
[26] Y. Tanimura, J. Phys. Soc. Jpn. **75**, 082001 (2006).
[27] T. Kato and Y. Tanimura, J. Chem. Phys. **117**, 6221 (2002).
[28] T. Kato and Y. Tanimura, J. Chem. Phys. **120**, 260 (2004).
[29] K. Okumura, A. Tokmakoff, and Y. Tanimura, J. Chem. Phys. **111**, 492 (1999).
[30] K. Okumura, D. M. Jonas, and Y. Tanimura, Chem. Phys. **266**, 237 (2001).
[31] K. Okumura and Y. Tanimura, J. Phys. Chem. A **107**, 8092 (2003).
[32] H.-D. Kim and Y. Tanimura, J. Chem. Phys. **123**, 224310 (2005).
[33] K. Kwac, H. Lee, and M. Cho, J. Chem. Phys. **120**, 1477 (2004).
[34] H. Torii, J. Phys. Chem. A **110**, 4822 (2006).
[35] A. Piryatinski, C. P. Lawrence, and J. L. Skinner, J. Chem. Phys. **118**, 9672 (2003).
[36] A. Goj and R. F. J. Loring, Chem. Phys. **124**, 194101 (2006).
[37] T. Hayashi and S. Mukamel, J. Chem. Phys. **125**, 194510 (2006).
[38] K. Kwac, C. Lee, Y. Jung, J. Han, K. Kwak, J. Zheng, M. D. Fayer, and M. Cho, J. Chem. Phys. **125**, 244508 (2006).
[39] M. F. DeCamp, L. P. DeFlores, J. M. McCracken, A. Tokmakoff, K. Kwac, and M. Cho, J. Phys. Chem. B **109**, 11016 (2005).
[40] K. Kwak, S. Park, and M. D. Fayer, Proc. Natl. Acad. Sci. U.S.A. **104**, 14221 (2007).
[41] B. Auer, R. Kumar, J. R. Schmidt, and J. L. Skinner, Proc. Natl. Acad. Sci. U.S.A. **104**, 14215 (2007).
[42] A. Ma and R. M. Stratt, Phys. Rev. Lett. **85**, 1004 (2000).
[43] A. Ma and R. M. Stratt, J. Chem. Phys. **116**, 4962 (2002).
[44] S. Saito and I. Ohmine, Phys. Rev. Lett. **88**, 207401 (2002).
[45] S. Saito and I. Ohmine, J. Chem. Phys. **119**, 9073 (2003).
[46] C. Dellago and S. Mukamel, J. Chem. Phys. **119**, 9344 (2003).
[47] Y. Nagata and Y. Tanimura, J. Chem. Phys. **124**, 024508 (2006).
[48] Y. Nagata, Y. Tanimura, and S. Mukamel, J. Chem. Phys. **126**, 204703 (2007).
[49] R. DeVane, B. Space, A. Perry, C. Neipert, C. Ridley, and T. Keyes, J. Chem. Phys. **121**, 3688 (2004).
[50] R. DeVane, C. Ridley, B. Space, and T. Keyes, J. Chem. Phys. **119**, 6073 (2003).
[51] S. Saito and I. Ohmine, J. Chem. Phys. **125**, 084506 (2006).
[52] T. I. C. Jansen, J. G. Snijders, and K. Duppen, J. Chem. Phys. **113**, 307 (2000).
[53] T. I. C. Jansen, J. G. Snijders, and K. Duppen, J. Chem. Phys. **114**, 10910 (2001).
[54] T. I. C. Jansen, K. Duppen, and J. G. Snijders, Phys. Rev. B **67**, 134206 (2003).
[55] R. DeVane, B. Space, T. I. C. Jansen, and T. Keyes, J. Chem. Phys. **125**, 234501 (2006).
[56] T. Hasegawa and Y. Tanimura, J. Chem. Phys. **125**, 074512 (2006).
[57] Y. Nagata, T. Hasegawa, and Y. Tanimura, J. Chem. Phys. **124**, 194504 (2006).
[58] Y. J. Yan and S. Mukamel, Phys. Rev. A **41**, 6485 (1990).
[59] Y. Tanimura and S. Mukamel, J. Phys. Chem. **97**, 12596 (1993).
[60] M. W. Johnson, E. Sandor, and E. Arzi, Acta Crystallogr. **B31**, 1998 (1975).
[61] R. J. Cole, J. Chem. Phys. **59**, 1545 (1973).
[62] I. Sheft and A. J. J. Perkins, J. Inorg. Nucl. Chem. **38**, 665 (1976).
[63] B. Desbat and P. V. Huong, J. Chem. Phys. **78**, 6377 (1983).
[64] S. Izvekov and G. A. Voth, J. Phys. Chem. B **109**, 6573 (2005).
[65] U. Röthlisberger and M. Parrinello, J. Chem. Phys. **106**, 4658 (1997).
[66] S. Mukamel, *Principles of Nonlinear Optical Spectroscopy* (Oxford University Press, Oxford, 1995).
[67] E. Wigner, Phys. Rev. **40**, 749 (1932).
[68] R. Kubo, J. Phys. Soc. Jpn. **19**, 2127 (1964).
[69] D. J. Evans and G. P. Morriss, *Statistical Mechanics of Nonequilibrium Liquids* (Academic, London, 1990).
[70] T. Keyes, D. Kivelson, and J. P. McTague, J. Chem. Phys. **55**, 4096 (1971).
[71] B. M. Ladanyi, Chem. Phys. Lett. **121**, 351 (1985).
[72] J. S. Muenter, J. Chem. Phys. **56**, 5409 (1972).
[73] S. M. Bass, R. L. DeLeon, and J. S. Muenter, J. Chem. Phys. **86**, 4305 (1987).
[74] A. Dullweber, B. Leimkuhler, and R. McLachlan, J. Chem. Phys. **107**, 5840 (1997).
[75] G. Martyna, M. Tuckerman, D. Tobias, and M. Klein, Mol. Phys. **87**, 1117 (1996).
[76] T. Steffen and Y. Tanimura, J. Phys. Soc. Jpn. **69**, 3115 (2000).
[77] Y. Tanimura and T. Steffen, J. Phys. Soc. Jpn. **69**, 4095 (2000).
[78] K. Okumura and Y. Tanimura, Phys. Rev. E **56**, 2747 (1997).
[79] M. Cho, G. R. Fleming, S. Saito, I. Ohmine, and R. M. Stratt, J. Chem. Phys. **100**, 6672 (1994).
[80] F. Fernandez-Alonso, S. E. McLain, J. W. Taylor, F. J. Bermejo, I. Bustinduy, M. D. Ruiz-Martin, and J. F. C. Turner, J. Chem. Phys. **126**, 234509 (2007).